



6th International Conference on Silicon Photovoltaics, SiliconPV 2016

PC1Dmod 6.2 – Improved simulation of c-Si devices with updates on device physics and user interface

Halvard Haug^{a*}, Johannes Greulich^b

^a Institute for Energy Technology (IFE), Institutstveien 18, 2007 Kjeller, Norway

^b Fraunhofer Institute for Solar Energy Systems (ISE), Heidenhofstraße 2, 79110 Freiburg, Germany

Abstract

In this paper we present a new update to PC1Dmod, which extends the original PC1D program by implementing Fermi-Dirac statistics and a range of state-of-the-art models in order to improve the accuracy of c-Si device simulation. In PC1Dmod 6.2 the list of models is further expanded to include a parameterization of incomplete ionization of dopants (Altermatt et al., J. Appl. Phys. 100, 113715, 2006), with parameters for phosphorus, boron, arsenic, gallium and aluminum. The results have been verified against a previous implementation of the model. We show that the inclusion of incomplete ionization is of particular importance for moderately doped surface regions with doping densities in the range $\sim 5 \times 10^{17}$ to $\sim 5 \times 10^{19} \text{ cm}^{-3}$, resulting in a deviation of up to 15% in the simulated recombination current density and sheet resistance. The effect of incomplete ionization is also shown to be more pronounced in devices made from compensated Si material. Furthermore, the default solar spectrum has also been updated in PC1Dmod 6.2, taking advantage of the increased maximum file size to include a more realistic representation. The generation profiles calculated using PC1Dmod 6.2 together with input from OPAL 2 agree well with results from Sentaurus TCAD for both planar and pyramidally textured surfaces, thus facilitating a more direct comparison between PC1Dmod 6.2 and other simulation programs utilizing standard spectra. The simulation comparison is also extended to the electrical performance of the modeled devices, showing good agreement in the calculated short-circuit current density for a range of planar and textured solar cells with varying emitter doping. Finally, several new output options, including emitter saturation current and injection-dependent lifetime curves have been added, enabling a simpler and more direct way for users to access and plot important device properties.

© 2016 The Authors. Published by Elsevier Ltd.

Peer review by the scientific conference committee of SiliconPV 2016 under responsibility of PSE AG.

Keywords: Device simulation; PC1D; dopant ionization; solar spectrum; emitter recombination; carrier lifetime

* Corresponding author. Tel.: +47 99 48 67 57, E-mail address: halvard.haug@ife.no

1. Introduction and overview of PC1Dmod development

PC1D is an efficient, one-dimensional semiconductor device simulator which is commonly used in solar cell research, teaching and engineering [1], [2]. The program is very fast and features an intuitive user interface and a large range of both input parameters and different output options. The carrier statistics in PC1D 5.9 is based on the Boltzmann approximation, and several PV-specific models have been developed for use in this framework. However, Fermi-Dirac (F-D) statistics should generally be used together with a correct model for the band structure and the density of states to obtain correct simulation results, particularly in highly doped regions like solar cell emitters. In our previous work on this subject, the physics engine of PC1D was updated in order to implement F-D statistics [3]. This was firstly done for a simplified, command line version of the program, which was called cmd-PC1D 6.0. We also implemented several advanced Si-specific models into cmd-PC1D 6.0 in order to improve the accuracy of simulations of c-Si devices, including models for carrier mobility [4], [5], Auger recombination [6], [7], electrical band gap and density of states [8], intrinsic carrier density [9], [10] and band gap narrowing (BGN) [11]. Later, the new physics were also implemented in an updated version of the original user interface, named PC1Dmod 6.1 [12]. This version also included a recently published, empirical BGN model [13], [14], an option for depth-dependent Shockley-Read Hall recombination and a comprehensive model for carrier mobility in compensated Si material [15].

In this work we continue to expand the list of model options by implementing the parameterization of Altermatt *et al.* for incomplete ionization of dopants [16], [17]. The implementation for all previous models has been verified against other, established simulation programs, and this has also been done in this case. The program is also provided with an updated, more detailed solar spectrum, and the resulting generation rates and short-circuit current values are compared with Sentaurus TCAD. Furthermore, the front surface recombination parameters can now be set as a function of the surface dopant concentration using the parameterization given in Ref. [18]. Finally, several new output options including the injection-dependent carrier lifetime, emitter saturation current density and sheet resistance are added. Easier access to these results provides less experienced users with a better understanding of the simulated device, and such values might in many cases also be used as direct input to 2D and 3D simulations based on the conductive boundary approach, like Quokka 2 [19]. With this update, we expect that PC1Dmod will continue to produce relevant simulation results with further improved accuracy and accessibility, and facilitate the use of advanced c-Si models in the PV community.

2. Incomplete ionization of dopants

The performance of crystalline silicon (c-Si) devices is greatly influenced by the equilibrium carrier concentrations of electrons (n_0) and holes (p_0), both in the base and in highly doped surface regions like solar cell emitters or back surface fields (BSFs). For uncompensated p-type Si p_0 is normally set to be equal to the acceptor dopant density N_A , thus assuming that all dopants are ionized. However, when the Fermi level E_F is close to the dopant energy level E_{dop} , a significant fraction of the dopant levels are occupied, and the resulting incomplete ionization (i.i.) should therefore often be taken into account. In PC1Dmod 6.2 we have implemented the well-accepted model for i.i. published by Altermatt *et al.* in 2006 [16], [17], which is based on a combination of theory and experimental data for P, B and As from the literature. It is worth noting that this i.i. is not describing the fraction of electrically active dopants in substitutional lattice sites, and is therefore not used to describe e.g. dopant activation of high concentrations of phosphorus and the solubility limit of dopant atoms in Si.

For a correct quantification of i.i., E_{dop} needs to be known as a function of the doping density N_{dop} , as E_{dop} approaches the band edge at high doping levels due to the so-called metal-insulator transition, leading to almost complete ionization at the highest dopant densities [16]. For the device implementation in PC1Dmod 6.2, we have chosen to use the recommended set of simplified equations assuming a discrete dopant energy level, given in Ref. [17]. The fraction of ionized dopants is then described as a function of the carrier densities n and p instead of the Fermi level, simplifying the computation:

$$\frac{N_D^+}{N_D} = 1 - \frac{b \cdot n}{n + g \cdot n_1}, \quad \frac{N_A^-}{N_A} = 1 - \frac{b \cdot p}{p + g \cdot p_1} \quad (1)$$

Here, g is the degeneracy factor (1/2 for donor levels and 1/4 for acceptor levels) and the parameter b depends on N_{dop} as

$$b = \frac{1}{1 + (N_{dop}/N_b)^d}. \quad (2)$$

n_1 and p_1 are statistical factors determined by E_{dop}

$$n_1 = N_C \exp\left(-\frac{E_{dop}}{kT}\right), \quad p_1 = N_V \exp\left(-\frac{E_{dop}}{kT}\right), \quad (3)$$

which in turn is a function of N_{dop} , parameterized as

$$E_{dop} = \frac{E_{dop,0}}{1 + (N_{dop}/N_{ref})^c}. \quad (4)$$

The i.i. of each type of dopant is thus described by the six parameters $E_{dop,0}$, N_{ref} , c , N_b , d and g , which have been adapted to give the best description of experimental data in each case. These parameters are listed in Table 1 for five common dopants. In addition to P, B and As, which were investigated in [16] and [17], we have also included recently published values for Al [20] and Ga [21]. For the device simulation the user can specify whether i.i. should be included and which dopants to use through the configuration file. Several iterations of the calculation are performed for the equilibrium case, in order to reach a consistent set of values which satisfy both charge neutrality $p + N_D^+ = n + N_A^-$ and the law of mass action $pn = n_i^2$. The i.i. calculation is also performed at each iteration, thus also taking into account the effect of excess carriers. The simulated fraction of ionized dopants as a function of the total dopant density is shown for each dopant type in Fig. 1(a). Note that Al and Ga both have rather high values for $E_{dop,0}$, and the degree of i.i. is therefore more pronounced for these dopants. When simulating the Al-BSF it has been shown that i.i. has a significant effect on the simulated saturation current density $J_{0,p+}$ of these regions [20], [22]. For the case of Ga dopants, it should be noted that Ref [21] only provides values for $E_{dop,0}$, N_{ref} , c and g and therefore only specifies the behavior of the curve up to the insulator-metal transition, that is before the turning point where the fraction of ionized dopants starts to increase towards unity at the highest doping levels. We therefore only show the simulated data for Ga up to $N_{dop} = 1 \times 10^{18} \text{ cm}^{-3}$. In order to avoid the unphysical behavior of a monotonically decreasing fraction of ionized Ga dopants at higher N_{dop} the values for boron-doped silicon (Si:B) has been used for N_b and d (dotted line in Fig. 1a), but users should be warned that i.i. calculations for Ga above this level will be less accurate.

Table 1. List of parameters used together with Eqs. (1)-(4) to describe i.i. of various dopants in c-Si

Dopant		Si:P	Si:As	Si:B	Si:Al	Si:Ga
Ref.		[17]	[17]	[17]	[20]	[21]
$E_{dop,0}$	(meV)	45.5	53.7	44.39	69.0	72.0
N_{ref}	(cm^{-3})	3×10^{18}	4×10^{18}	1.7×10^{18}	5.4×10^{18}	5×10^{18}
c		2	1.5	1.4	3	0.75
N_b	(cm^{-3})	6×10^{18}	1.4×10^{19}	6×10^{18}	5.5×10^{18}	*
d		2.3	3	2.4	2.6	*
g		1/2	1/2	1/4	1/4	1/4

* Parameters not used in Ref. [21], and they are therefore here set equal to the values for Si:B. These parameters mainly affect the i.i. above the metal insulator transition $N_A \approx 10^{18} \text{ cm}^{-3}$, and results using Ga dopants are therefore highly uncertain at high dopant concentrations above this level.

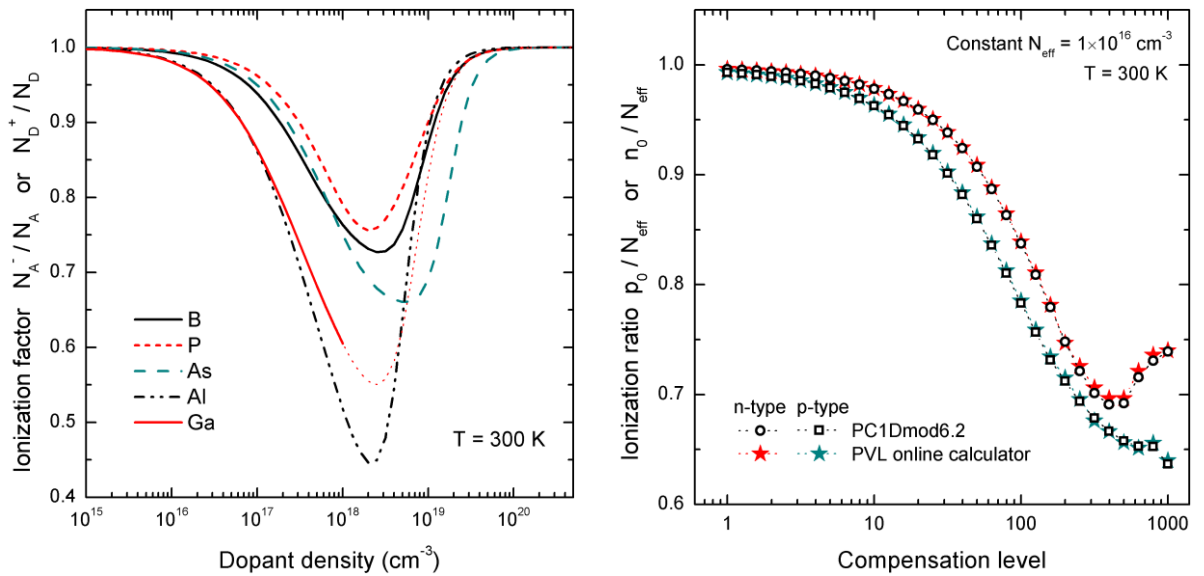


Fig.1. (a) Ratio of ionized dopants as a function of total dopant concentration for B, P and As, Al and Ga. The published parameterization for Ga is only given for N_{dop} below the metal-insulator transition, as indicated by the solid red line. (b) Ionization ratio, defined as the ratio between the equilibrium majority carrier concentration and the effective doping, as a function of compensation level in the material. For a fixed effective doping, the error caused by assuming complete ionization of dopants increases with increasing compensation level up to the point where the dopant concentrations become larger than N_{crit} . Data are shown both from PC1Dmod and an online dopant ionization calculator, showing excellent agreement.

Another common example where i.i. plays an important role is in compensated Si materials. This may be an unintuitive result, as compensation doping moves the Fermi level towards the middle of the band gap, and for p-type material the addition of donor atoms thus *increases* the fraction of ionized acceptors in the material. However, if one considers the fact that the effective doping $N_{\text{eff}} = N_A - N_D$ in many cases is much smaller than the acceptor concentration, a given fraction of non-ionized acceptors will have a much larger impact on the carrier density for the compensated case [23]. The relevant quantity is therefore not N_A^- / N_A , but the ionization ratio, i.e. the ratio between the equilibrium carrier density and the effective doping, p_0 / N_{eff} . This quantity thus also describes the error that is made by assuming that all dopants are ionized. Fig. 1(b) shows the ionization ratio for both n- and p-type compensated c-Si material as a function of the compensation level $C_l = (N_A + N_D) / N_{\text{eff}}$, using a combination of B and P dopants. The ionization ratio decreases with increasing compensation level up to the point where the two doping concentrations pass the metal-insulator transition, which occurs at a high compensation level of $C_l \sim 300\text{-}500$ in this case. We also use these simulations to verify that the i.i. model has been implemented correctly, by comparing the results with those obtained by an online dopant ionization calculator [24] which uses a different implementation of the same i.i. model. Note that the i.i. model of Ref. [17] is derived for uncompensated material. The dopant energy from the band edge decreases with increasing doping density primarily due to the interaction between the dopant atoms and is only secondarily influenced by screening by free carriers. Therefore, we assume that in compensated materials each dopant energy level only depends on the density of its own dopant species. However, we should keep in mind that adding a second dopant species in similar concentration may affect both dopant energies. As discussed in [23], a recent study showed no changes in the dopant energy levels for B and P in compensated material with dopant concentrations up to $1 \times 10^{17} \text{ cm}^{-3}$, and there is very little data in the literature for higher doping levels. We therefore use the i.i. model of Ref. [17] also for compensated material, but caution should be taken for high dopant concentrations.

3. Updated solar spectrum file

When PC1D 5.9 was released in 1997, the maximum length for external files was limited to 200 lines in order to speed up the simulation as much as possible. These computational limitations are not as relevant on modern computers, and in PC1Dmod 6.1 the maximum number of elements was increased for several aspects of the program, including an increase in the maximum file length, which is now arbitrarily set to 1000 lines. This allows us to include a new, default solar spectrum file with improved resolution and a higher level of detail as shown in Fig. 2(a). The new AM1.5g default spectrum file is obtained from the IEC norm [25]. The spectral range of 300 to 4000 nm is evenly sampled in 5 nm wavelength intervals, since a finer resolution doesn't significantly increase the accuracy for typical solar cell setups. E.g. for devices with 70 nm SiN_x anti-reflection coating (ARC), textured or planar front and 150 μm wafer thickness, the generation rate J_{ph} for the 5 nm interval differs less than 0.01 mA/cm² from that of the 1 nm interval. Since PC1Dmod is intended primarily for silicon single junction devices, steep edges in the quantum efficiency are not as relevant as e.g. for III-V multi-junction solar cells, where an even finer resolved spectrum can be beneficial. By changing the default optical excitation file PC1Dmod simulations will be more comparable to those obtained using other simulation tools, including OPAL 2 [26], Wafer ray tracer [27], OPTOS [28], [29] and Sentaurus TCAD [30].

In order to illustrate the improvement in precision and to validate the correctness of the implementation of the new spectrum, optical simulations performed with PC1Dmod and Sentaurus TCAD are compared. Two device structures are simulated, one with a planar and one with an alkaline textured front side (3 μm pyramid height). An 80 nm thin SiN_x layer with refractive index $n = 2.03$ [31] is applied. In PC1Dmod, the front surface reflection (including parasitic absorption in the ARC) is provided as an external file calculated with OPAL 2. The assumed wafer thickness is 180 μm. Since the models for internal reflection of PC1Dmod and Sentaurus TCAD are different, a rear reflection of zero is assumed in both cases in order to get a high comparability of the two tools. The cumulated generation profiles are shown in Fig. 2(b), along with their relative deviation from each other. PC1Dmod correctly simulates a larger generation rate for the textured case compared to the planar case, in accordance with expectations and Sentaurus TCAD. The deviations of the two tools are below 1% for the planar case and for generation at depths larger than 0.1 μm. The integration of Sentaurus' generation profile to a cumulated generation profile is done with best care by integration of a logarithmic interpolation function. Nevertheless, the generation profile is extremely steep in the first nano- and micrometres (more than double-exponential). Thus, it is likely that the integration causes the increase of the deviations for smaller depths. For the textured case, deviations of approximately 10% are obtained for depths up to 10 μm and a close match for larger depths. This deviation is probably caused by the different ways of the two tools to generate a one-dimensional generation rate for the three-dimensional pyramidal geometry. Concerning the total generation rate or generated current density J_{ph} , again a close match is obtained with the updated spectrum ($\Delta J_{ph,planar} = 0.001\%$, $\Delta J_{ph,textured} = -0.089\%$). With the original spectrum of PC1D 5.9, deviations from Sentaurus TCAD are significantly larger ($\Delta J_{ph,planar} = -0.50\%$, $\Delta J_{ph,textured} = -0.65\%$).

In order to further validate the new spectrum, the comparison of PC1Dmod with Sentaurus TCAD is extended to the electrical performance of the simulated devices. Using the above generation profiles, we apply a variation of Gaussian-shaped P-doped emitters with surface concentrations between 1×10^{18} and 2.56×10^{20} cm⁻³ with standard deviation of the Gaussian profiles of 0.2 μm. The surface recombination velocity S_{p0} is chosen depending on the surface doping concentration according to the parameterization of Kimmerle *et al.* [32]. The base ($N_A = 10^{16}$ cm⁻³) is assumed to be limited by Auger recombination, and the rear surface recombination velocity is set to 100 cm/s. The resulting short-circuit current densities J_{sc} and the relative deviations are shown in Fig. 3. The difference between textured and planar case is reproduced again by the two tools. Furthermore, the decrease of J_{sc} with increasing surface doping concentration is reproduced accurately. For peak doping concentrations below 10^{20} cm⁻³ the deviations are smaller than 0.4%. For the planar case, the deviations are approximately 0.2% for all peak doping concentrations.

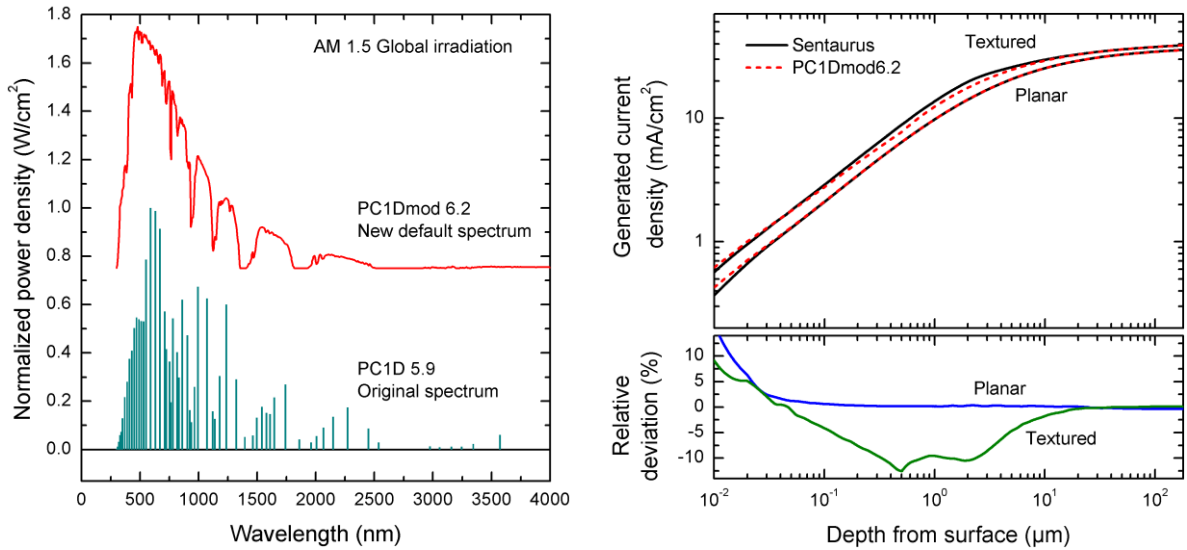


Fig. 2. (a) Comparison of the AM1.5g solar spectrum previously used as default in PC1D (bottom) and the updated spectrum used as standard in PC1Dmod 6.2 (top). The increased maximum file size for external files allows for a much more finely resolved and evenly spaced spectrum (5 nm). Note that PC1D defines the spectrum as the power density (W/cm^2) and not the spectral density ($\text{W}/\text{cm}^2/\text{nm}$), so the unevenly spaced original spectrum is best represented by a bar graph. The generated current density calculated using a selected solar cell model is indicated for each case. (b) Cumulative generation rate as a function of depth, simulated for both planar and textured surfaces using PC1Dmod 6.2 and Sentaurus TCAD. External files calculated with OPAL were used to account for front reflectance in the PC1Dmod simulations. Bottom: Relative deviation in the generation profiles calculated using PC1Dmod6.2, as compared to those obtained by Sentaurus simulations.

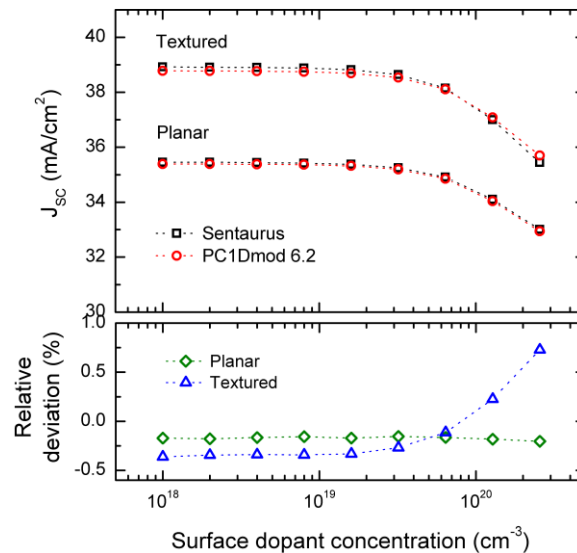


Fig.3. Short-circuit current density simulated using the updated AM1.5g spectrum for a series of solar cells with increasing surface dopant concentration. PC1Dmod 6.2 simulations were compared with those obtained using Sentaurus TCAD, showing a good agreement both for planar and pyramidal textured surfaces.

4. New output options

In addition to the changes in device physics and input data described in the sections above, version 6.2 also has included some new options for the program outputs in the result section, in the graph view and in batch mode. Firstly, the main current-voltage curve parameters which are commonly calculated by many PC1D users manually

are now directly accessible, including the short-circuit current density, the fill factor, the current and voltage at the maximum power point and the maximum power density in mW/cm^2 (which in most cases corresponds to cell efficiency in %). Secondly, much of the previous development in the device physics of PC1Dmod (F-D statistics, BGN, mobility, etc.) has largest impact on the simulation results for highly doped regions. It is therefore natural to also include a possibility to directly output the saturation current density J_{0e} at diffused junctions. The emitter simulation results (J_{0e} , sheet resistance ρ_{sheet} and junction depth x_j) are available when using a specific excitation file, which sets the junction under a moderate forward bias of 0.55 V in the dark. For a p-type substrate, J_{0e} is then calculated from the hole recombination current density J_p at a depth x_e using the same procedure used in the dedicated emitter recombination tool EDNA 2 [33]:

$$J_{0e} = \frac{J_p(x_e)}{n(x_e) \cdot p(x_e) - n_{i,eff}^2(x_e)} n_{i,eff}^2(x_e). \quad (5)$$

Here, $n_{i,eff}$ is the effective intrinsic carrier density (including BGN) and x_e is the depth corresponding to the edge of the emitter side of the space charge region, taken as the point where $n_0(x_e) = 10 \times N_A$, where N_A is the acceptor base doping.

An example of J_{0e} simulations using PC1Dmod 6.2 is given in Fig. 4(a), showing the simulated J_{0e} and ρ_{sheet} for a series of emitters with varying surface dopant concentration N_{surf} , with the same device model as shown in Fig. 3 above. In both cases we have taken advantage of the new possibility to include a parameterization for S_{p0} as a function of N_{surf} , using the parameters from Kimmerle *et al.* [32]. This means that all the data points in the graph could be produced in two simple batch simulations, with and without the i.i. model enabled. As seen in the figure, the incomplete ionization model clearly affects the results for $N_{surf} < \sim 5 \times 10^{19} \text{ cm}^{-3}$, with an up to 15% relative deviation in the simulated values for the lower range of doping densities around $1 - 5 \times 10^{18} \text{ cm}^{-3}$. The same simulations were also performed using EDNA 2, resulting in less than 1% relative deviation from PC1Dmod for all the data points, with a typical deviation of approximately 0.2% (not shown).

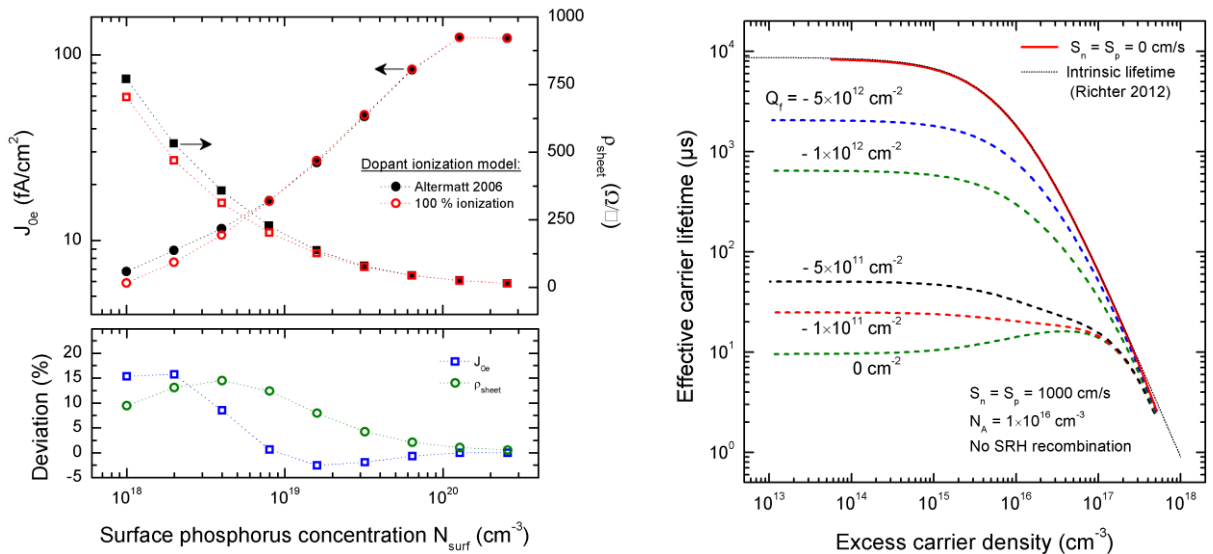


Fig.4. (a) Top: Simulated emitter saturation current density J_{0e} (left axis) and emitter sheet resistance ρ_{sheet} (right axis) for a series of Gaussian emitter profiles with varying surface phosphorus concentration and a fixed depth factor. Bottom: Relative deviation in the calculated values using the incomplete ionization model in Refs. [15], [16] as compared to the case of 100% dopant ionization. (b) Injection-dependent lifetime curves simulated in PC1Dmod 6.2 using a transient simulation with gradually varying light intensity. The new version of the program includes automatic calculation of such curves.

Finally, because PC1D has the ability to perform transient simulations, it is also suited for simulating injection-dependent lifetime characteristics that can be measured using the quasi steady state photoconductance (QSSPC) technique, another important topic for Si solar cell research and development. In PC1Dmod 6.2, this simulation is coded into the program in such a way that the user is able to directly output the effective carrier lifetime as a function of the excess minority carrier density for a given lifetime sample. These calculations are also used together with a dedicated excitation file setting up the transient lifetime measurement, with secondary files specifying the light pulse and the flash spectrum. An example of such simulations is given in Fig. 4 (b), showing lifetime curves for a symmetrical, homogeneously boron-doped ($N_A = 10^{16} \text{ cm}^{-3}$) lifetime sample including surface recombination, but without bulk Shockley-Read-Hall (SRH) recombination for different values for the surface charges in the passivation layer. Note that when SRH recombination is disabled both for the surfaces and the bulk of the wafer the result corresponds to the intrinsic recombination curve of the Si material, in this case the parameterization given in Ref. [6], which is used as the default model in PC1Dmod. With this functionality, PC1Dmod 6.2 offers the possibility to not only calculate the injection-dependent Auger lifetime or SRH lifetime, but also a combination of Auger, radiative, bulk SRH and surface SRH including the effect of surface charges and the depth-dependent variations of the carrier densities.

5. Summary

In this paper we have presented version 6.2 of PC1Dmod and cmd-PC1D, with updates in physical models (incomplete ionization of dopants), external files (new AM1.5g spectrum) and in the input and output options available to the user (parameterization of surface recombination, automatic simulation of the saturation current density and sheet resistance, plotting of injection-dependent lifetime curves, etc). PC1Dmod 6.2 and cmd-PC1D 6.2 are freely available for download and are currently hosted by PV Lighthouse (<http://www.pvlighthouse.com.au/>). The source code for the two programs has now been merged into a single project, which will be available at www.sourceforge.net.

Acknowledgements

The authors want to thank Pietro Altermatt and Heiko Steinkemper for fruitful discussion on device simulation of incomplete ionization and Erik Stensrud Marstein for valuable feedback and proofreading. Funding for this work was partly provided by the Norwegian Research Council and Elkem Solar AS through the EnergiX program.

References

- [1] D. A. Clugston and P. A. Basore. PC1D version 5: 32-bit solar cell modeling on personal computers. Conference Record of the Twenty-Sixth IEEE Photovoltaic Specialists Conference, 1997; pp. 207–210.
- [2] P. A. Basore. Numerical modeling of textured silicon solar cells using PC-1D. IEEE Transactions on Electron Devices, 1990; vol. 37, no. 2, pp. 337–343.
- [3] H. Haug, A. Kimmerle, J. Greulich, A. Wolf, and E. Stensrud Marstein. Implementation of Fermi–Dirac statistics and advanced models in PC1D for precise simulations of silicon solar cells. Sol. Energy Mater. Sol. Cells, 2014; vol. 131, no. 0, pp. 30–36.
- [4] D. B. M. Klaassen. A unified mobility model for device simulation—I. Model equations and concentration dependence, Solid. State. Electron., 1992; vol. 35, no. 7, pp. 953–959.
- [5] D. B. M. Klaassen. A unified mobility model for device simulation—II. Temperature dependence of carrier mobility and lifetime, Solid. State. Electron., 1992; vol. 35, no. 7, pp. 961–967.
- [6] A. Richter, S. W. Glunz, F. Werner, J. Schmidt, and A. Cuevas. Improved quantitative description of Auger recombination in crystalline silicon. Phys. Rev. B, 2012; vol. 86, no. 16, p. 165202.
- [7] M. J. Kerr and A. Cuevas. General parameterization of Auger recombination in crystalline silicon. J. Appl. Phys., 2002; vol. 91, no. 4, pp. 2473–2480.
- [8] M. A. Green. Intrinsic concentration, effective densities of states, and effective mass in silicon. J. Appl. Phys., 1990; vol. 67, no. 6, p. 2944.
- [9] P. P. Altermatt, A. Schenk, F. Geelhaar, and G. Heiser. Reassessment of the intrinsic carrier density in crystalline silicon in view of band-gap narrowing. J. Appl. Phys., 2003; vol. 93, no. 3, p. 1598.
- [10] A. B. Sproul and M. A. Green. Intrinsic carrier concentration and minority-carrier mobility of silicon from 77 to 300 K. J. Appl. Phys., vol. 1993; 73, no. 3, p. 1214.

- [11] A. Schenk. Finite-temperature full random-phase approximation model of band gap narrowing for silicon device simulation. *J. Appl. Phys.*, 1998; vol. 84, no. 7, p. 3684.
- [12] H. Haug, J. Greulich, A. Kimmerle, and E. S. Marstein. PC1Dmod 6.1 – state-of-the-art models in a well-known interface for improved simulation of Si solar cells. *Sol. Energy Mater. Sol. Cells*, 2015; vol. 142, pp. 47–53.
- [13] D. Yan and A. Cuevas. Empirical determination of the energy band gap narrowing in highly doped n+ silicon. *J. Appl. Phys.*, 2013; vol. 114, no. 4, p. 044508.
- [14] D. Yan and A. Cuevas. Empirical determination of the energy band gap narrowing in p+ silicon heavily doped with boron. *J. Appl. Phys.*, 2014; vol. 116, no. 19, p. 194505.
- [15] F. Schindler, M. Forster, J. Broisch, J. Schön, J. Giesecke, S. Rein, W. Warta, and M. C. Schubert. Towards a unified low-field model for carrier mobilities in crystalline silicon. *Sol. Energy Mater. Sol. Cells*, 2014; vol. 131, pp. 92–99.
- [16] P. P. Altermatt, A. Schenk, and G. Heiser. A simulation model for the density of states and for incomplete ionization in crystalline silicon. I. Establishing the model in Si:P. *J. Appl. Phys.*, 2006; vol. 100, no. 11, p. 113714.
- [17] P. P. Altermatt, A. Schenk, B. Schmihüsen, and G. Heiser. A simulation model for the density of states and for incomplete ionization in crystalline silicon. II. Investigation of Si:As and Si:B and usage in device simulation. *J. Appl. Phys.*, 2006; vol. 100, no. 11, p. 113715.
- [18] P. P. Altermatt, J. O. Schumacher, A. Cuevas, M. J. Kerr, S. W. Glunz, R. R. King, G. Heiser, and A. Schenk. Numerical modeling of highly doped Si:P emitters based on Fermi–Dirac statistics and self-consistent material parameters. *J. Appl. Phys.*, 2002; vol. 92, no. 6, p. 3187.
- [19] A. Fell. A Free and Fast Three-Dimensional/Two-Dimensional Solar Cell Simulator Featuring Conductive Boundary and Quasi-Neutrality Approximations. *IEEE Transactions on Electron Devices*, 2013; vol. 60, no. 2, pp. 733–738.
- [20] H. Steinkemper, M. Rauer, P. Altermatt, F. D. Heinz, C. Schmiga, and M. Hermle. Adapted parameterization of incomplete ionization in aluminum-doped silicon and impact on numerical device simulation. *J. Appl. Phys.*, 2015; vol. 117, no. 7, p. 074504.
- [21] M. Forster, A. Cuevas, E. Fourmond, F. E. Rougieux, and M. Lemiti. Impact of incomplete ionization of dopants on the electrical properties of compensated p-type silicon. *J. Appl. Phys.*, 2012; vol. 111, no. 4, p. 043701.
- [22] Y. Chen, H. Shen, and P. P. Altermatt. Analysis of recombination losses in screen-printed aluminum-alloyed back surface fields of silicon solar cells by numerical device simulation. *Sol. Energy Mater. Sol. Cells*, 2014; vol. 120, pp. 356–362.
- [23] M. Forster, F. E. Rougieux, A. Cuevas, B. Dehestre, A. Thomas, E. Fourmond, and M. Lemiti. Incomplete Ionization and Carrier Mobility in Compensated p-Type and n-Type Silicon. *IEEE J. Photovoltaics*, 2013; vol. 3, no. 1, pp. 108–113.
- [24] PV Lighthouse dopant ionisation calculator [Online]. Available: https://www2.pvlighthouse.com.au/calculators/dopant_ionisation_calculator/dopant_ionisation_calculator.aspx.
- [25] IEC 60904-3. Photovoltaic devices - part 3: measurement principles for terrestrial photovoltaic (PV) solar devices with reference spectral irradiance data, 2nd ed., International Electrotechnical Commission, 2008.
- [26] K. R. McIntosh and S. C. Baker-Finch. OPAL 2: Rapid optical simulation of silicon solar cells. 38th IEEE Photovoltaic Specialists Conference (PVSC), 2012; pp. 265–271.
- [27] Wafer ray tracer. [Online]. Available: https://www2.pvlighthouse.com.au/calculators/wafer_ray_tracer/wafer_ray_tracer.html.
- [28] J. Eisenlohr, N. Tucher, O. Höhn, H. Hauser, M. Peters, P. Kiefel, J. C. Goldschmidt, and B. Bläsi. Matrix formalism for light propagation and absorption in thick textured optical sheets. *Opt. Express*, 2015; vol. 23, no. 11, pp. A502–A518.
- [29] N. Tucher, J. Eisenlohr, P. Kiefel, O. Höhn, H. Hauser, M. Peters, C. Müller, J. C. Goldschmidt, and B. Bläsi. 3D optical simulation formalism OPTOS for textured silicon solar cells. *Opt. Express*, 2015; vol. 23, no. 24, pp. A1720–A1734.
- [30] Synopsis Inc. Sentaurus Device, Version H-2013.03.
- [31] S. Duttgupta, F. Ma, B. Hoex, T. Mueller, and A. G. Aberle. Optimised Antireflection Coatings using Silicon Nitride on Textured Silicon Surfaces based on Measurements and Multidimensional Modelling. *Energy Procedia*, 2012; vol. 15, pp. 78–83.
- [32] A. Kimmerle, M. Momtazur Rahman, S. Werner, S. Mack, A. Wolf, A. Richter, and H. Haug. Precise parameterization of the recombination velocity at passivated phosphorus doped surfaces. *J. Appl. Phys.*, 2016; vol. 119, no. 2, p. 025706.
- [33] K. R. McIntosh and P. P. Altermatt. A freeware 1D emitter model for silicon solar cells. in 35th IEEE Photovoltaic Specialists Conference, 2010; pp. 002188–002193.